

# High energy muons in extensive air showers

C. Gámez\*, M. Gutiérrez, J.S. Martínez, M. Masip

*CAFPE and Departamento de Física Teórica y del Cosmos  
Universidad de Granada, E-18071 Granada, Spain*

car,mgg,jsilverio,masip@ugr.es

## Abstract

The production of very high energy muons inside an extensive air shower is observable at  $\nu$  telescopes and sensitive to the composition of the primary cosmic ray. Here we discuss five different sources of these muons: pion and kaon decays; charmed hadron decays; rare decays of unflavored mesons; photon conversion into a muon pair; and photon conversion into a  $J/\psi$  vector meson decaying into muons. We solve the cascade equations for a  $10^{10.5}$  GeV proton primary and find that unflavored mesons and gamma conversions are the two main sources of  $E \geq 10^{8.5}$  GeV muons, while charm decays dominate at  $10^{5.5} \text{ GeV} < E < 10^{8.5} \text{ GeV}$ . In inclined events one of these muons may deposit a large fraction of its energy near the surface, implying anomalies in the longitudinal profile of the shower and in the muon to electron count at the ground level. In particular, we show that 1 out of 330 proton showers of  $10^{10.5}$  GeV will include an  $E > 10^7$  GeV deposition within  $500 \text{ g/cm}^2$ . We also show that the production of high energy muons is very different in proton, iron or photon showers. In particular, conversions  $\gamma \rightarrow \mu^+ \mu^-$  are the main source of  $E \geq 10^4$  GeV muons in photon showers.

---

\*Now at CIEMAT, Avenida Complutense 22, E-28040 Madrid, Spain

# 1 Introduction

Extensive air showers (EASs) initiated by ultrahigh energy cosmic rays (CRs) include millions of collisions and decays of secondary particles. These showers can be observed with fluorescence detectors, able to *count* the number of charged particles produced as the shower develops along the atmosphere, and/or surface detectors, which register energy depositions of the particles reaching the ground. Despite the large number of processes involved in an individual EAS, its dynamics can be understood within the following simplified scheme [1].

Let us take a proton primary facing a relatively large slant depth (*e.g.*,  $X \approx 2000 \text{ g/cm}^2$  from a zenith angle  $\theta_z \approx 60^\circ$ ). The first interaction will take place high in the atmosphere, after the proton has crossed a hadronic interaction length ( $\lambda_{\text{int}} \approx 41 \text{ g/cm}^2$  at  $E = 10^{10} \text{ GeV}$ ). It will result into a leading baryon carrying around 25% of the initial energy plus dozens of light mesons (mostly pions) sharing the rest of the energy. The leading baryon will interact again deeper into the atmosphere, but after just four collisions 99% of its energy will already be transferred to pions. High energy charged pions, in turn, may collide giving more pions of lower energy or they may decay into leptons,  $\pi^+ \rightarrow \mu^+ \nu_\mu$ . Decays are only favoured at relatively low energies, below (with a strong dependence on the altitude) 50 GeV, so the production of very high energy muons and neutrinos is suppressed. In contrast, neutral pions of all energies decay almost instantly ( $\pi^0 \rightarrow \gamma\gamma$ ) giving photons that feed the electromagnetic (EM) component of the EAS. Photons will convert into  $e^+e^-$  pairs after  $9X_0/7 \approx 47 \text{ g/cm}^2$ , whereas electrons will radiate half their energy after a similar depth, so the EM energy is transformed fast into a large number of lower-energy particles that define the shower maximum at  $X_{\text{max}} \approx 800 \text{ g/cm}^2$ . The precise position of  $X_{\text{max}}$  has fluctuations  $\Delta X_{\text{max}} \approx 50 \text{ g/cm}^2$  that depend basically on the inelasticity in the first few collisions of the leading baryon. Notice also that most of the energy in the EAS will be processed through gammas and electrons instead of muons and neutrinos: although the three pion species are created at a similar rate, high-energy charged pions tend to collide giving both charged and neutral pions, whereas all the energy that goes into neutral pions becomes EM and has a small return to hadrons. In inclined events, after a depth around  $2X_{\text{max}}$  most gammas and electrons have been absorbed by the atmosphere and the signal becomes dominated by muons, although it includes an EM *tail* created by muon radiative depositions and muon decays.

Within this simple picture, the value of  $X_{\text{max}}$  or the signal at the surface detectors depend critically on the inelasticity (fraction of energy lost by the leading hadron) and the multiplicity (number of secondary hadrons that share that energy) in nucleon and pion collisions in the air. Unfortunately, the study of these two observables at colliders is not

easy, as it involves a very wide range of energies and a kinematical region (ultraforward) of difficult access.<sup>†</sup> The uncertainty that they introduce could possibly explain the apparent excess (around a 50%) in the number of muons at the ground level recently emphasized by the Pierre Auger Observatory [3]. Nevertheless, the picture provides a good description of the main features in an EAS. The different values of  $X_{\max}$  for proton or iron primaries, for example, are easily understood if one sees a nucleus shower as the superposition of  $A$  nucleon showers of energy  $E/A$ , each one with a smaller value of  $X_{\max}$ .

However, there are a few features in an EAS that are in principle observable and require a more elaborate scheme. The production of  $E \geq 10^5$  GeV neutrinos is one of them: It is expected that at those energies pion and kaon decays become a less effective source of neutrinos than charmed hadron decays [4, 5]. Another one are the muons of also very high energy. The weak decays of light mesons produce both muons and neutrinos, but muons may also appear with no neutrinos in the EM decays of unflavored mesons or in the interactions of high energy photons with atmospheric nuclei [6, 7]. These relatively rare processes are often not included in the Monte Carlo simulation of an air shower, in particular, charmed hadrons or the decays of unflavored mesons into muon pairs have just been added to SIBYLL 2.3C [8] but are absent in EPOS-LHC [9]. Our main objective in this work is to understand and compute the production of high energy muons inside an EAS.

In addition to probe the production of charm and unflavored mesons in high energy collisions, we find two phenomenological reasons why these most energetic muons may be interesting. First, they could be useful in composition studies. Obviously, an iron shower will never contain a muon carrying a fraction of energy larger than  $1/A = 0.017$ ; but how frequent are muons with, for example, a 0.1% of the shower energy? It turns out that such muons are 10 times more likely in a proton than in an iron EAS. They will often appear in pairs, in the core of the shower, always accompanied by a bundle of lower energy muons. Their inclination when they cross a neutrino telescope and/or catastrophic energy losses there would reveal the minimum energy of these muons [10–12]. A second reason of interest is the possibility of anomalies in the longitudinal development of an inclined ( $\theta_z \geq 60^\circ$ ) EAS: One of these muons may start a  $10^7$  EM shower at 100–600 g/cm<sup>2</sup> from the ground (when most of the energy has already been absorbed by the atmosphere), changing substantially the signal at the surface detectors.

The plan of this article is as follows. In the next section we review the different processes that may produce high energy muons inside an EAS. In section 3 we solve the cascade equations for the average  $10^{10.5}$  GeV proton, iron or gamma shower and we deduce the spectrum

---

<sup>†</sup>A forward spectrometer at the LHC appears indeed as a very promising possibility [2].

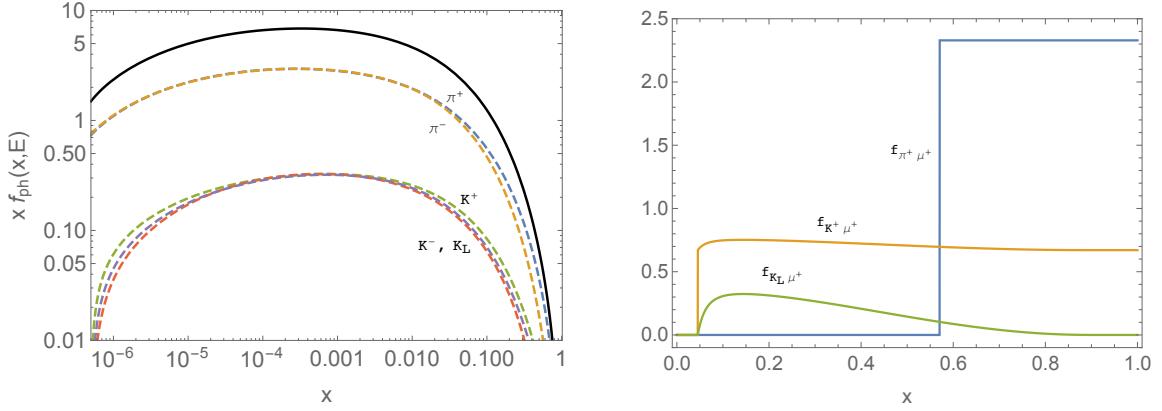


Figure 1: Pion and kaon yields in proton-air collisions at  $10^6$  GeV (left) and muon yields in pion and kaon decays (right).

of muons reaching the ground from large zenith inclinations. In section 4 we parametrize the three main radiative processes experienced by a muon in the air (bremsstrahlung, pair production and photonuclear collisions) and we estimate the probability for a large energy deposition near the surface. Finally, we conclude in section 5.

## 2 Muon production channels

(i) *Conventional muons from pion and kaon decays.*

We have obtained a fit<sup>‡</sup> for the yields  $f_{hh'}(x, E)$  of hadrons  $h' = p, n, \bar{p}, \bar{n}, \pi^\pm, K^\pm, K_L$  produced in the collisions of nucleons, pions and kaons of energy  $E$  with an average air nucleus ( $x = E_{h'}/E$ ). In particular, the four lowest moments provided by our fits,

$$Z_{hh'}(n, E) = \int_0^1 dx x^n f_{hh'}(x, E), \quad (1)$$

match the ones derived from  $5 \times 10^4$  collisions simulated with EPOS-LHC at different energies. In Fig.1-left we show for illustration the yields of light mesons in proton-air collisions at  $10^6$  GeV. Notice that the zero moment of  $f_{hh'}(x, E)$  corresponds to the total number of particles  $h'$  created per collision, whereas the first moment is the fraction of energy taken by these particles. In the example, the average collision produces 52.9 charged pions and 7.9 kaons that take respectively 34.6% and 7.1% of the proton energy. Using SIBYLL [13] we obtain similar results: 51.6 charged pions and 8.5 kaons carrying 30.7% and 7.6% of the proton energy, respectively. The yields in pion and kaon collisions are analogous.

<sup>‡</sup>The details about these fits will be presented elsewhere.

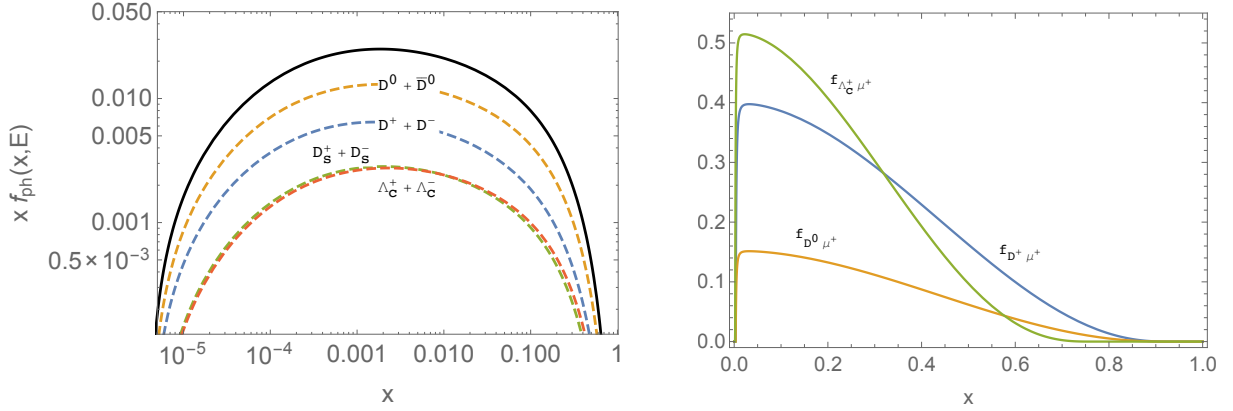


Figure 2: Left: Charmed-hadron yields in proton-air collisions at  $10^6$  GeV obtained with SIBYLL [13]. Right: Muon yields in charmed hadron decays.

The decay of these light mesons will produce muons [14]. In Fig. 1–right we have included the decay yields  $f_{h\mu}(x, E)$  in the ultrarelativistic limit, with the zero moment giving the branching ratio into muons in these decays.

(ii) *Muons from charmed-hadron decays.*

SIBYLL has recently incorporated charmed-hadron production: in Fig. 2 we plot for illustration the yields in proton collisions at  $10^6$  GeV. It is remarkable that these yields incorporate the so called *forward* charm [15–17], *i.e.*, charm quarks that combine with a valence quark in the projectile and, as a result, fragment into a charmed hadron carrying a large fraction  $x$  of the collision energy (notice that this effect is not included in the usual perturbative calculations [18]).

Once produced the  $D$  mesons and  $\Lambda_c$  baryons may decay giving muons (see the decay yields also in Fig. 2 [7]). However, at  $E \geq 10^6$  GeV they may also collide losing part of their energy. The inelasticity  $K = 1 - \langle x \rangle$  in charmed hadron collisions with air is smaller than in pion or proton collisions [19, 20], in particular, we will assume a gaussian distribution with  $\langle x \rangle = 0.56$  for the fraction of energy carried by the leading charmed hadron after a collision with an air nucleus (versus just  $\langle x \rangle = 0.26$  for the leading pion in a  $10^6$  GeV pion collision).

(iii) *Muons from the rare decays of unflavored mesons.*

The unflavored mesons  $\eta$ ,  $\rho$ ,  $\omega$ ,  $\eta'$  and  $\phi$ , with masses between 0.5 and 1 GeV, include decay channels with muon pairs. For example,  $\text{BR}(\eta \rightarrow \mu^+ \mu^- \gamma) = 3.1 \times 10^{-4}$  or  $\text{BR}(\phi \rightarrow \mu^+ \mu^-) = 2.9 \times 10^{-4}$  [21]. These decay modes are more rare than in  $D$ -meson decays (*e.g.*,  $\text{BR}(D^+ \rightarrow \bar{K}^0 \mu^+ \nu_\mu) = 0.092$ ), but this is partially compensated by the smaller mass and then the larger frequency of unflavored mesons in hadronic collisions. Moreover, they always

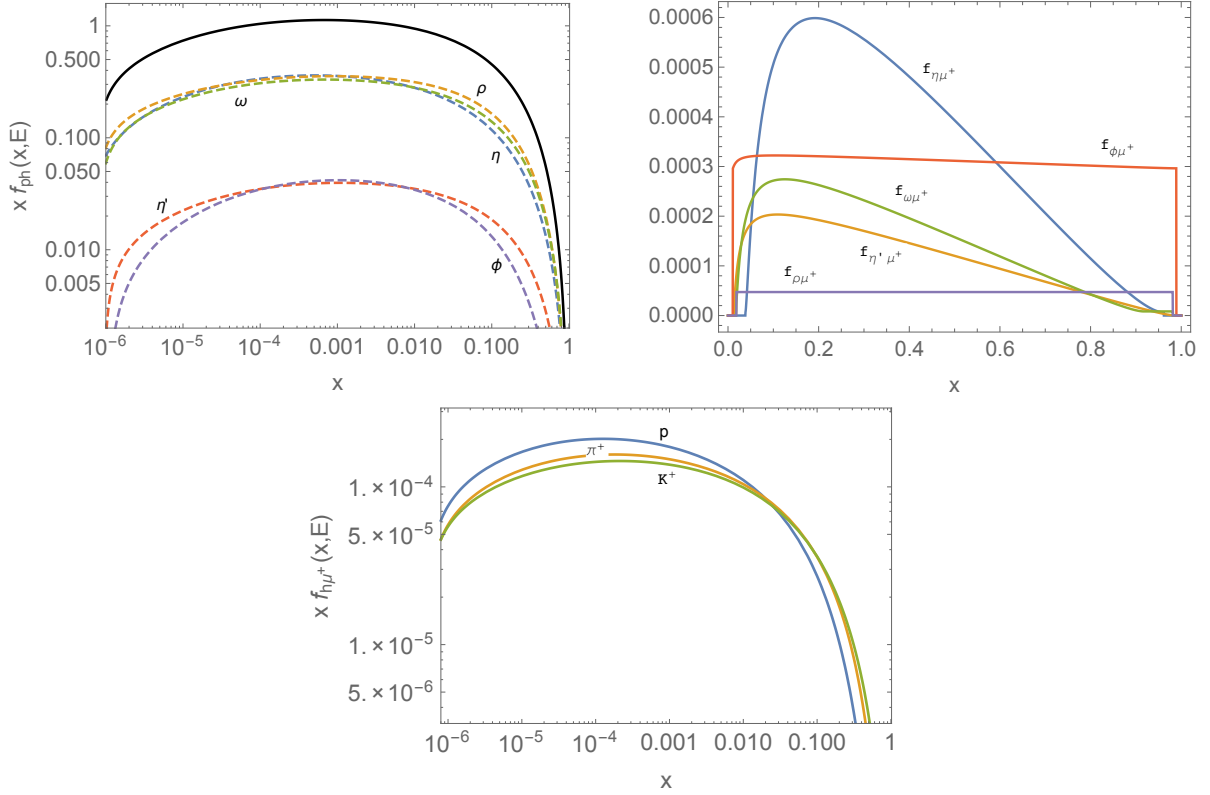


Figure 3: Unflavored meson yield in proton-air collisions at  $10^6$  GeV (left), muon yield in their decays (right), and muon yield through unflavored mesons in proton, pion and kaon collisions with air at  $10^6$  GeV (lower).

decay promptly, whereas most  $D$  mesons and  $\Lambda_c$  baryons of  $E > 10^7$  GeV collide in the air and lose energy instead of decaying.

In Fig. 3 we plot the yields of unflavored mesons in proton-air collisions at  $10^6$  GeV together with their decay yields into muons [7]. Since they decay almost instantly, we can obtain the muon yield in hadron collisions through unflavored mesons as

$$f_{h\mu}(x, E) = \int_x^1 dx' \frac{1}{x'} \sum_{h'=\eta, \rho, \dots} f_{hh'}(x', E/x) f_{h'\mu}(x/x'). \quad (2)$$

We include for illustration also in Fig. 3 the muon yield in proton, pion and kaon collisions with air at  $10^6$  GeV.

(iv) *Photon conversion into a muon pair.*

High energy photons appear in hadron collisions mostly through  $\pi^0$  and  $\eta$  decays. We obtain with EPOS-LHC that photons take 20.6% of the energy in proton-air collisions at  $10^6$  GeV, and that this percentage is even larger in pion and kaon collisions (24.4% and 24.1%,

respectively). The gamma conversion length into  $e^+e^-$  pairs is then  $\lambda_\gamma^{ee} = X_0/(7/9 - b/3)$ , with  $X_0 = 37.1 \text{ g/cm}^2$  and (in air)  $b = 0.012$ , whereas the conversion into muon pairs will be suppressed by a factor of  $m_e^2/m_\mu^2$ ,  $\lambda_\gamma^{\mu\mu} \approx 2 \times 10^6 \text{ g/cm}^2$ . The fraction of energy going to each muon is distributed [22]

$$f_{\gamma\mu^+}(x) = \frac{\lambda_\gamma^{\text{int}}(E)}{X_0} \left( \frac{m_e}{m_\mu} \right)^2 \left( \frac{2}{3} - \frac{b}{2} + \left( \frac{4}{3} + 2b \right) \left( x - \frac{1}{2} \right)^2 \right). \quad (3)$$

This is then a very rare process ( $m_e^2/m_\mu^2 = 2.4 \times 10^{-5}$ ) but one where all the photon energy goes into muons.

(v) *Photon conversion into a vector meson decaying into muons.*

In the previous process the photon fluctuates into a virtual muon pair that goes on shell after an EM interaction with an air nucleus. However, the photon may also fluctuate into a  $q\bar{q}$  pair, *i.e.*, a virtual vector meson that becomes real after a hadronic (pomeron mediated) interaction with the nucleus. This fluctuation is less likely due to the larger mass of the meson, but the suppression is partially compensated by the larger coupling in the hadronic process.

It turns out that in 1 out of 400 collisions (and even more often at low energies near a hadronic resonance) the photon behaves like a rho meson. The most frequent photonuclear collision is then an inelastic process resulting into a multiplicity of pions, but over 10% of them are exclusive ( $\gamma p \rightarrow \rho p$ ) or dissociative ( $\gamma p \rightarrow \rho X$ ) conversions where the  $\rho$  meson gets almost all of the photon energy. We will also consider the  $\gamma$  conversion into a  $J/\psi$  meson (a  $c\bar{c}$  state), more rare than the  $\rho$  (specially at lower energies) but with a much larger branching ratio into  $\mu^+\mu^-$  (around a 5.9%).

In our estimate for these processes we have extrapolated the HERA observations at  $\sqrt{s} < 300 \text{ GeV}$  [23, 24] up to  $\sqrt{s} < 300 \text{ TeV}$  using a two-pomeron scheme:

$$\begin{aligned} \sigma_{\text{tot}}(\gamma p) &= 69.0 s^{0.08} + 175 s^{-0.60}, \\ \sigma(\gamma p \rightarrow \rho p) &= 4.9 s^{0.11} + 21 s^{-0.40}, \\ \sigma(\gamma p \rightarrow J/\psi p) &= 0.0016 s^{0.41}, \end{aligned} \quad (4)$$

where  $s$  is given in  $\text{GeV}^2$  and the cross sections in  $\mu\text{b}$ . To include dissociative conversions [25, 26] we have just added a 60% to the exclusive cross sections above, and we have assumed that the scaling to go from a proton to a nucleus target coincides with the one in pion collisions.

### 3 Cascade equations and muon flux

We will solve numerically the (longitudinal) cascade equations for 15 hadron species  $h$  ( $p$ ,  $n$ ,  $\bar{p}$ ,  $\bar{n}$ ,  $\pi^\pm$ ,  $K^\pm$ ,  $K_L$ ,  $D^\pm$ ,  $D^0$ ,  $\bar{D}^0$ ,  $D_s^\pm$ ,  $\Lambda_c^\pm$ ), photons, electrons and muons, with  $\mu^\pm$  from the prompt decay of unflavored mesons included in the yields  $f_{h\mu}(x, E)$  and  $f_{\gamma\mu}(x, E)$  (see previous section). The generic equations are [14]

$$\begin{aligned} \frac{d\Phi_i(E, t)}{dt} = & -\frac{\Phi_i(E, t)}{\lambda_i^{\text{int}}(E)} - \frac{\Phi_i(E, t)}{\lambda_i^{\text{dec}}(E, t)} + \sum_{j=h, \gamma, e} \int_0^1 dx \frac{f_{ji}(x, E/x)}{x} \frac{\Phi_j(E/x, t)}{\lambda_j^{\text{int}}(E/x)} + \\ & \sum_{k=h} \int_0^1 dx \frac{f_{ki}^{\text{dec}}(x, E/x)}{x} \frac{\Phi_k(E/x, t)}{\lambda_j^{\text{dec}}(E/x, t)}, \end{aligned} \quad (5)$$

where  $\Phi_i = dN_i/dE$ ,  $t$  is the slant depth and the interaction/decay lengths are expressed in  $\text{g}/\text{cm}^2$ . We will focus on particles with energy between 1 TeV and the energy of the primary.

The EM component of the shower will be started in hadronic collisions through the decay of neutral mesons and other hadronic resonances (we obtain  $f_{h\gamma}(x, E)$  from a fit to EPOS-LHC simulations); we neglect the production of electrons in hadron and muon decays and also the photonuclear collisions of electrons. The cascade equations for photons and electrons read then [1]

$$\begin{aligned} \frac{d\Phi_\gamma(E, t)}{dt} = & -\frac{\Phi_\gamma(E, t)}{\lambda_\gamma^{\text{int}}(E)} + \sum_{j=h} \int_0^1 dx \frac{f_{j\gamma}(x, E/x)}{x} \frac{\Phi_j(E/x, t)}{\lambda_j^{\text{int}}(E/x)} \\ & + \int_0^1 dx \frac{f_{e\gamma}(x, E/x)}{x} \frac{\Phi_e(E/x, t)}{\lambda_e^{\text{int}}(E/x)}, \end{aligned} \quad (6)$$

and

$$\begin{aligned} \frac{d\Phi_e(E, t)}{dt} = & -\frac{\Phi_e(E, t)}{\lambda_e^{\text{int}}(E)} + \int_0^1 dx \frac{2 f_{\gamma e}(x, E/x)}{x} \frac{\Phi_\gamma(E/x, t)}{\lambda_\gamma^{\text{int}}(E/x)} \\ & + \int_0^{1-x_{\min}} dx \frac{f_{e\gamma}(1-x, E/x)}{x} \frac{\Phi_e(E/x, t)}{\lambda_e^{\text{int}}(E/x)}, \end{aligned} \quad (7)$$

where  $x_{\min}(E) = E_{\min}^\gamma/E$  and we have used that  $f_{ee}(x, E) = f_{e\gamma}(1-x, E)$ . The interaction lengths are

$$\begin{aligned} \frac{1}{\lambda_\gamma^{\text{int}}(E)} &= \frac{7-3b}{9X_0} \left(1 + \frac{m_e^2}{m_\mu^2}\right) + \frac{\sigma_{\gamma A}^{\text{had}}}{m_A}; \\ \frac{1}{\lambda_e^{\text{int}}(E)} &= \frac{\int_{x_{\min}}^1 dx \phi(x)}{X_0}, \end{aligned} \quad (8)$$

with  $m_A$  the target mass (in grams) in an average hadronic collisions in the air (*i.e.*,  $A = 14.6$ ), while the EM yields are [22]

$$f_{\gamma e}(x, E) = \frac{\lambda_\gamma^{\text{int}}(E)}{X_0} \psi(x); \quad \psi(x) = \frac{2}{3} - \frac{b}{2} + \left(\frac{4}{3} + 2b\right) \left(x - \frac{1}{2}\right)^2,$$



$$f_{e\gamma}(x, E) = \frac{\lambda_e^{\text{int}}(E)}{X_0} \phi(x); \quad \phi(x) = x + \frac{1-x}{x} \left( \frac{4}{3} + 2b \right), \quad (9)$$

We obtain the nuclear cross sections needed in the hadronic interaction lengths ( $\lambda_h^{\text{int}} = m_A/\sigma_{hA}$ ) with EPOS-LHC, and we use isospin symmetry to deduce the whole set of yields from the ones in  $p$ ,  $\pi^+$  and  $K^+$  collisions. As for the muons, we neglect energy loss as they propagate, but in the next section we will calculate the probability for a catastrophic energy deposition in the air near the surface. For the atmosphere we assume [27] (in  $\text{g}/\text{cm}^3$ )

$$\rho(h) = \begin{cases} 1.210 \times 10^{-10} (44.33 - h)^{4.253}, & h < 11 \text{ km}; \\ 2.053 \times 10^{-3} \exp\left(-\frac{h}{6.344 \text{ km}}\right), & h > 11 \text{ km}. \end{cases} \quad (10)$$

We have taken 200 logarithmic bins of energy and 2500 linear bins of altitude with  $h_0 = 70 \text{ km}$ , and we have checked that the transport through the atmosphere conserves the total energy in the shower. Our results are summarized in Fig. 4. There we plot the particle flux (number of particles per unit energy) at the ground level for several primaries, all of them with  $E = 10^{10.5} \text{ GeV}$ .

The upper figures include a proton from zenith angles  $\theta_z = 60^\circ$  (left) and  $\theta_z = 0^\circ$  (right). We find a total of 0.0065 muons with  $E \geq 10^8 \text{ GeV}$  in the first case and 0.0052 muons in a vertical shower. This implies, respectively, that around 1 in 150 or 1 in 190 showers include such a muon. The contribution to this muon count from unflavored mesons and gamma conversions is basically independent from the shower inclination, while the charm contribution has a 40% reduction for vertical showers (it goes from 0.0030 to 0.0018). In the inclined proton shower charm decays generate 46% of the  $E > 10^8 \text{ GeV}$  muons, unflavored decays 30% and photon conversions 23%, being the contribution from  $\gamma \rightarrow \mu^+\mu^-$  three times larger than the one from  $\gamma \rightarrow J/\psi \rightarrow \mu^+\mu^-$ .

In the lower figures we plot the fluxes for iron (left) or photon (right) showers of also  $E > 10^{10.5} \text{ GeV}$ , both from a zenith inclination  $\theta_z = 60^\circ$ . The number of muons with energy  $E > 10^8 \text{ GeV}$  is, respectively, 0.0010 and 0.0052. This means that only 1 in 1000 iron showers or 1 in 190 photon showers include such a muon. In an iron primary charm decays contribute a 28% to this muon count, whereas in gamma showers 99% of the muons come from gamma conversions (71% in EM interactions and 28% through  $J/\psi$  decays). We also see that the conventional contribution from pion and kaon decays is negligible both for proton or gamma primaries, but it is more significant (2.1%) in iron showers. We find remarkable that in photon showers the conversions  $\gamma \rightarrow \mu^+\mu^-$  and  $\gamma \rightarrow J/\psi \rightarrow \mu^+\mu^-$  give many more muons than pion and kaon decays even at lower energies (see the discussion on muons from inelastic photonuclear collisions in [28]).

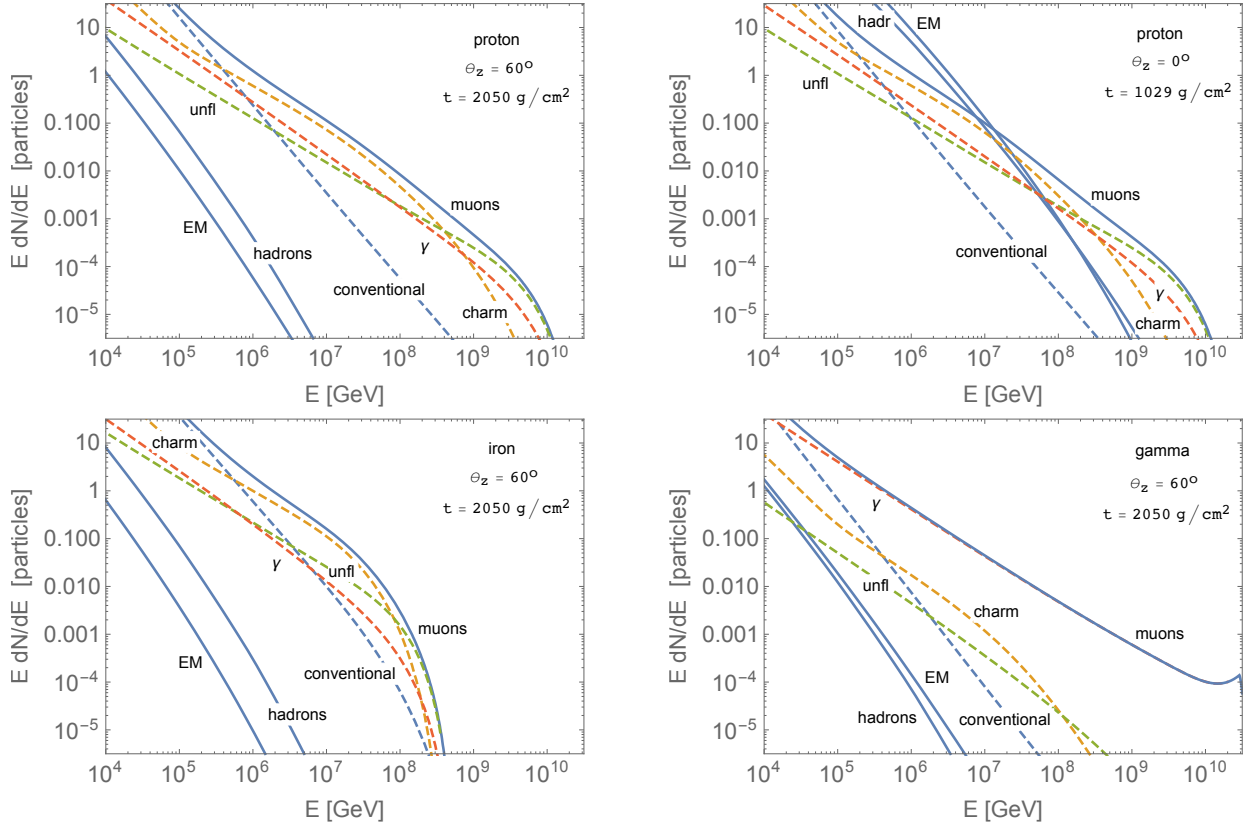


Figure 4: Particle count at the ground level for a  $10^{10.5}$  GeV proton (top left), iron nucleus (bottom left) or gamma ray (bottom right) coming from  $\theta_z = 60^\circ$ , and for a vertical proton of the same energy (top right). The EM line includes photons and electrons, and the dashed lines indicate the different contributions to the muon flux (the  $\gamma$  line includes the muons from  $\gamma \rightarrow \mu\mu$  and from  $\gamma \rightarrow \rho, J/\psi \rightarrow \mu\mu$ ).

## 4 Muon energy depositions near the surface

High-energy muons may radiate a significant fraction of their energy through three different processes: bremsstrahlung, pair production or photonuclear interactions [29]. The first two processes would start an EM shower, whereas photonuclear collisions would define a hadronic sub-shower. In inclined events these energy depositions could occur very deep in the atmosphere, when most of the shower energy has been absorbed. In Fig. 5 we plot the differential cross section for these radiative processes, being  $\nu$  the fraction of the muon energy deposited in the air.

The probability that a muon of energy  $E$  has an interaction within a depth  $\Delta X = 500$

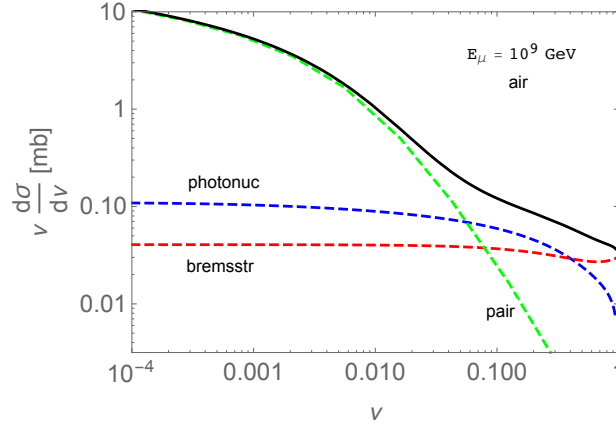


Figure 5: Cross section to deposit a fraction  $\nu$  of energy in muon collisions in the air.

$\text{g}/\text{cm}^2$  where it radiates a minimum energy  $E_0$  is

$$p(E_0, E) = \frac{\Delta X}{m_A} \int_{E_0/E}^1 d\nu \frac{d\sigma}{d\nu}, \quad (11)$$

with values larger than 1 expressing the average number of depositions. For an incident flux  $\Phi_\mu(E)$  the probability to have the same type of energy deposition is then

$$p(E_0) = \frac{\Delta X}{m_A} \int_{E_0}^{\infty} dE \Phi_\mu(E) \int_{E_0/E}^1 d\nu \frac{d\sigma}{d\nu}. \quad (12)$$

Our results for the 3 primaries considered in the previous section are the following. In a  $10^{10.5}$  GeV proton shower from  $\theta_z = 60^\circ$  the probability to have an energy deposition above  $10^7$  GeV is 0.0030, *i.e.*, we can expect such an anomaly in one per 330 proton showers. The same anomaly would occur in only 1 out of 7000 iron showers. In photon showers the spectrum of high-energy muons is much harder than in hadron showers (see Fig. 4). Since a  $10^9$ – $10^{10}$  GeV muon loses around 0.4% of its energy per  $1000 \text{ g}/\text{cm}^2$  of air, *most* muons in this energy range (appearing in around 1 in 200 photon showers) will start  $O(10^7 \text{ GeV})$  EM mini-showers near the ground.

## 5 Summary and discussion

In studies of EASs the connection between the primary CR and the secondary particles observable at the surface usually relies on a Monte Carlo simulation. It is then necessary to make sure that all the relevant effects are included. We have shown that to account for the most energetic muons in a shower one has to include, in addition to charmed hadrons, the rare decays of unflavored mesons and the photon conversions into muon pairs or  $J/\psi$  mesons.

This is clear in photon showers at all muon energies (these conversions produce many more muons than pion and kaon decays even at  $10^5$  GeV, see Fig. 4), but also in proton showers at  $E \geq 10^9$  GeV.

Our results are based on a numerical solution to the (longitudinal) cascade equations through the atmosphere. This method is usually applied to primary fluxes instead of a single particle, but we have shown that it can give accurate results also in this second case. Most important, the method is able to incorporate easily and precisely each one of the new effects. Our results are consistent with the ones in [8], that refer to the total atmospheric muon flux (not the muons inside an individual shower) and emphasize the relevance of unflavored meson decays.

We estimate that 1 in 150 inclined events started by a  $10^{10.5}$  GeV proton primary contain a muon of  $E > 10^8$  GeV, or that 1 in 300 proton showers include an anomalous radiative deposition of energy above  $10^7$  GeV at a slant depth within  $500 \text{ g/cm}^2$  near the surface. These frequencies are different for iron or gamma primaries. The appearance of such EM shower after most of the parent EAS has been absorbed (*i.e.*, beyond  $1500 \text{ g/cm}^2$ ) could introduce anomalies in the muon to electron count at the ground level [30], something that will be measured with accuracy after the upgrade in the surface detectors at AUGER [31]. These high energy muons could also be of interest at  $\nu$  telescopes. In particular, a determination of the atmospheric muon flux at  $E \geq 100$  TeV and its correlation with the neutrino flux at the same energies could reveal the production of forward charm in hadronic collisions.

Monte Carlo hadronic simulators like EPOS-LHC or SIBYLL give predictions at extreme energies, well beyond the ones achieved at particle colliders. The muons discussed here are a probe of those energies. We think that this could make them useful in the study of both the hadronic cross sections in this regime and the composition of the highest energy CRs.

## Acknowledgments

The authors would like to thank T. Pierog and R. Ulrich for providing the *Cosmic Ray Monte Carlo* package. This work has been supported by MICINN of Spain (FPA2016-78220) and by Junta de Andalucía (FQM101 and *Programa Operativo de Empleo Juvenil*). MG acknowledges an *Iniciación a la Investigación* fellowship from the University of Granada.

## References

- [1] T. K. Gaisser, “Cosmic rays and particle physics,” Cambridge, UK: Univ. Pr. (1990) 279 p.
- [2] M. Albrow, PoS EDSU **2018** (2018) 048 doi:10.22323/1.335.0048 [arXiv:1811.02047 [physics.ins-det]].
- [3] A. Aab *et al.* [Pierre Auger Collaboration], Phys. Rev. D **91** (2015) no.3, 032003 Erratum: [Phys. Rev. D **91** (2015) no.5, 059901].
- [4] P. Gondolo, G. Ingelman and M. Thunman, Astropart. Phys. **5** (1996) 309.
- [5] R. Enberg, M. H. Reno and I. Sarcevic, Phys. Rev. D **78** (2008) 043005.
- [6] J. I. Illana, M. Masip and D. Meloni, JCAP **0909** (2009) 008.
- [7] J. I. Illana, P. Lipari, M. Masip and D. Meloni, Astropart. Phys. **34** (2011) 663.
- [8] A. Fedynitch, F. Riehn, R. Engel, T. K. Gaisser and T. Stanev, “The hadronic interaction model Sibyll-2.3c and inclusive lepton fluxes,” arXiv:1806.04140 [hep-ph].
- [9] T. Pierog, I. Karpenko, J. M. Katzy, E. Yatsenko and K. Werner, Phys. Rev. C **92** (2015) 034906.
- [10] F. Tenholt *et al.* [IceCube Collaboration], “The IceCube Neutrino Observatory - Contributions to ICRC 2017 Part III: Cosmic Rays,” arXiv:1710.01194 [astro-ph.HE].
- [11] A. G. Bogdanov, R. P. Kokoulin, G. Mannocchi, A. A. Petrukhin, O. Saavedra, V. V. Shutenko, G. Trinchero and I. I. Yashin, Astropart. Phys. **98** (2018) 13.
- [12] A. A. Kochanov, A. D. Morozova, T. S. Sinegovskaya and S. I. Sinegovsky, J. Phys. Conf. Ser. **1181** (2019) no.1, 012054.
- [13] E. J. Ahn, R. Engel, T. K. Gaisser, P. Lipari and T. Stanev, Phys. Rev. D **80** (2009) 094003.
- [14] P. Lipari, Astropart. Phys. **1** (1993) 195.
- [15] S. J. Brodsky, P. Hoyer, C. Peterson and N. Sakai, Phys. Lett. **93B** (1980) 451.
- [16] F. Halzen and L. Wille, Phys. Rev. D **94** (2016) no.1, 014014.

- [17] F. Carvalho, A. V. Giannini, V. P. Goncalves and F. S. Navarra, Phys. Rev. D **96** (2017) no.9, 094002.
- [18] R. Gauld, J. Rojo, L. Rottoli, S. Sarkar and J. Talbert, JHEP **1602** (2016) 130.
- [19] R. Barcelo, J. I. Illana, M. D. Jenkins and M. Masip, Phys. Rev. D **83** (2011) 034027.
- [20] A. Bueno, A. Gascon, J. I. Illana and M. Masip, JCAP **1202** (2012) 028.
- [21] M. Tanabashi *et al.* [Particle Data Group], Phys. Rev. D **98** (2018) no.3, 030001.
- [22] B. Rossi and K. Greisen, Rev. Mod. Phys. **13** (1941) 240.
- [23] P. Merkel, “Diffractive photoproduction of heavy vector mesons at HERA,” DESY-THESIS-1999-030.
- [24] A. Aktas *et al.* [H1 Collaboration], Eur. Phys. J. C **46** (2006) 585.
- [25] S. Chekanov *et al.* [ZEUS Collaboration], Eur. Phys. J. C **26** (2003) 389.
- [26] D. Bendova, J. Cepila and J. G. Contreras, Phys. Rev. D **99** (2019) no.3, 034025.
- [27] K. Maeda, Fortsch. Phys. **21** (1973) 113.
- [28] F. Cornet, C. A. Garcia Canal, A. Grau, G. Pancheri and S. J. Sciutto, Phys. Rev. D **92** (2015) 114011.
- [29] D. E. Groom, N. V. Mokhov and S. I. Striganov, Atom. Data Nucl. Data Tabl. **78** (2001) 183.
- [30] C. A. García Canal, J. I. Illana, M. Masip and S. J. Sciutto, Astropart. Phys. **85** (2016) 50.
- [31] A. Aab *et al.* [Pierre Auger Collaboration], Nucl. Instrum. Meth. A **798** (2015) 172 doi:10.1016/j.nima.2015.06.058 [arXiv:1502.01323 [astro-ph.IM]].